Rational mutagenesis of Thermobifida fusca cutinase to modulate the enzymatic degradation of polyethylene terephthalate

Arpita Mrigwani[1], Madhav Pitaliya[1], Harman Kaur[1], Bhishem Thakur[1], and Purnananda Guptasarma[1]

[1]Indian Institute of Science Education and Research Mohali

July 8, 2022

Abstract

Thermobifida fusca cutinase (*Tf*C) is a carboxylesterase (CE) that degrades the environmental pollutant, polyethylene terephthalate (PET). *Tf*C also acts upon PET's degradation intermediates (DIs), such as oligoethylene terephthalate (OET), and bis-/mono-hydroxyethyl terephthalate (BHET/MHET), to convert these into terephthalic acid (TPA), the terminal product of PET degradation. We examined *Tf*C's surface, compared it to that of other CEs, and performed molecular docking and MD simulations with an OET, 2HE-(MHET) $_3$, to understand interactions between *Tf*C's surface and the OET, at *Tf*C's active site as well as vicinal regions. We mutated 17 residues on *Tf*C's surface, mostly individually, but sometimes using pairs of mutations, to see how these modulate *Tf*C's activity. Most mutants/variants showed a decrease in activity against solid PET. Some killed activity completely. However, three mutations (L90F, F209I and F249R), made using a background mutation (G62A) already reported to improve activity by almost ˜2.0-fold, yielded increases in activity that were between ˜1.3- and ˜2.0-fold higher than that of G62A *Tf*C (which we found to display a ˜1.7-fold increase in activity over *Tf*C, in our own experiments). *Tf*C variants, G62A/F249R, and G62A/F209I, exhibit the highest activities yet observed in any *Tf*C mutants/variants, against PET, and BHET, respectively.

Introduction

Since plastics emerged in the 1950s, over 8.3 billion metric tons of plastic have accumulated in the planet's ecosystems [Geyer et al., 2017], with PET being mainly responsible for this pollution [Ellis et al., 2021]. Clearly, an urgent need exists to develop both linear (valorisation-based) and circular (recycling-based) economies around PET degradation, to reduce carbon footprints created through inefficient PET degradation and production of PET from petrochemicals [Ru et al., 2020; Sarah and Gloria, 2021]. Degradation of PET by enzymatic means provides a 'green' route to breaking down solid plastic PET into pure terephthalic acid (TPA) using environmentally-friendly, low cost reactions [Kawai et al., 2019]. Thermostable cutinases (EC 3.1.1.74) and their structural homologs are enzymes that degrade aliphatic esters such as cutin (found upon leaf surfaces). Cutinases are now known to also hydrolyse ester bonds in PET chains, to release terephthalic acid (TPA), and various degradation intermediates (DIs) of PET such as oligoethylene terephthalate (OET) chains of varying lengths, bis-2-hydroxyethyl terephthalate (BHET), and mono-2-hydroxyethyl terephthalate (MHET) [Kawai et al., 2019]. Cutinases have also emerged as promising enzymes for hydrolysis of ester bonds in non-PET plastics such as polybutylene succinate, polyethylene furanoate, and polycaprolactone [Maurya et al., 2020].

The best enzymatic degradation reactions involving PET are carried out at (or near) PET's glass transition temperature (˜70 °C), which is the temperature at which chains become mobile and accessible to the active site(s) of thermophilic hydrolases [Kawai et al., 2020]. Of various thermophilic cutinases identified thus far, (i) metagenomically-derived leaf branch compost cutinase (LCC), (ii) *Humicola insolens* cutinase (HiC), and (iii) *Thermobifida fusca* cutinase (*Tf* C), are all capable of hydrolysing PET in the range of 60-70 °C [Kawai

et al., 2020]. In the present study, we engineered *Tf* C through a detailed examination of residues likely to contact PET. We compared *Tf* C with other PET hydrolases such as the thermostable cutinase, LCC [Sulaiman et al., 2012], and the meso-stable hydrolase, PETase, from *Ideonella sakaiensis*[Yoshida et al., 2016; Fecker et al., 2018]. In terms of amino acid sequences, *Tf* C displays 57.4 %, and 51 %, similarity, respectively, with LCC and PETase. All of these enzymes host a conserved GXSXG motif, a conserved catalytic triad of Ser-His-Asp residues, and an alpha-beta hydrolase fold [Buchholz et al., 2022].

Degradation of PET is coarsely described as repeating cycles of five successive kinetic steps: (i) enzyme binding to solid PET, through general hydrophobic interactions; (ii) enzyme binding to PET chain backbones, through involvement of active site(s); (iii) rearrangements in the covalent bonds of PET; (iv) release of product [which could be OET, BHET, MHET, or TPA, as well as ethylene glycol (EG)]; and (v) enzyme dissociation from solid PET [Wei et al., 2022]. Enzymes such as LCC or *Tf* C are required to bind to PET through attractive forces facilitating formation of enzyme-substrate complexes. According to Sabatier's principle, intermediate enzyme binding strength leads to most efficient degradation, since too low an affinity makes for weak enzyme-substrate complexes, as well as low rates of degradation, whereas too high an affinity makes for strong enzyme-substrate complexes, poor product/enzyme release, and poor turnover [Jensen et al., 2022]. Therefore, an intermediate binding affinity which is sufficient for enzyme-substrate complex formation is thought to be the best for high turnover. In search of a *Tf* C mutant/variant displaying higher turnover than *Tf* C, we describe below the obtaining of such mutants/variants through rational mutagenesis involving either (i) creation or reduction of space at the active site, or (ii) increase or decrease of hydrophobicity, at the active site, or vicinal to the active site.

2. Materials and methods:

2.1 Bioinformatics studies : Structural comparisons of *Tf* C with LCC and PETase were done using PYMOL (Schrödinger). Molecular docking and Molecular Dynamics simulation studies, respectively, were performed GLIDE (Schrödinger) and Desmond (Schrödinger), employing parameters described previously [Mrigwani et al., 2022]. Docking was performed using *Tf* C (PDB ID: 4CG1) and 2HE-$(MHET)_3$, containing three terephthalate moieties. Structural alignments were done using the Tm align web server [Zhang and Skolnick, 2005].

2.2 Cloning, expression and protein purification of wild type Tf C*and its mutants* : The gene encoding *Tf* C was amplified from the genomic DNA of *Thermobifida fusca* (MTCC No. 1754^{T}) and cloned between Bam HI and Hind III restriction sites in pQE-30 (Qiagen) for expression in fusion with an N-terminal 6xHis tag. *Tf* C variants/mutants were created through site directed mutagenesis of this gene through splicing by overlap extension PCR (SOE-PCR), prior to cloning into the same vector, between the same sites. All clones were transformed into XL1-Blue for constitutive expression. Transformed XL1-Blue cells (grown at 37 °C for 9 h at 220 rpm) were harvested and disrupted. Cell debris was separated through centrifugation at 12,000 rpm for 1 h, and lysates subjected to Ni-NTA (IMAC) chromatography. The second step of purification involved size exclusion chromatography (SEC) on a GE Superdex-75 Increase 10/300 GL column, run on a GE AKTA Purifier-10 workstation, using 25 mM sodium dihydrogen phosphate buffer of pH 8.0.

2.3 Circular dichroism (CD) studies : An MOS-500 CD spectrometer (BioLogic, France) was used to examine secondary structure in enzymes, using concentrations of 0.2 mg/ml, and a quartz cuvette of 2 mm path length. Mean Residue Ellipticity was calculated as MRE= (ϑ×mean residue weight×100)/(1000×concentration in mg/ml×pathlength in cm); where, ϑ is the raw ellipticity. For chemical and thermal kinetics, enzyme was incubated at various guanidium hydrochloride (Gdm.HCl) concentrations and temperatures for 2 h, with monitoring of CD spectral intensity at 222 nm. Folded fractions were determined and used to determine rates of unfolding and thermodynamic parameters of stability.

2.4 Differential Scanning Calorimetry (DSC) studies : Using VP-DSC (Microcal), thermal histories were created through repeated heating/cooling (10-15 up/down scans) at 90 °C/hr (upscan; 20-90°C) and 60 °C/hr (downscan; 90-20 °C). Then, buffer in the sample cell was replaced by 0.5 mg/ml. One cycle of up/down scans was performed to determine enzyme melting temperature, refolding ability and enthalpy associated

with unfolding, with raw data fitted using a non-2-state cursor init model (Microcal).

2.5 PET-binding and activity against PET/BHET : Prior to binding/activity assays, circular discs of commercial PET film (Goodfellow, Product code: GF25214475) were washed with 1% SDS, water and ethanol for 30 min, and air dried. For binding assays, 2 µM enzyme was incubated with PET for 40 h at 60 °C. Films were washed with buffer. Enzyme fractions in solution, or bound to PET (extracted through boiling with SDS-PAGE sample loading buffer) were determined through electrophoresis, and densitometry using Image lab software (Bio-Rad). For activity assays, films were incubated with 2 µM enzyme(s) at 60 °C for 50 h in phosphate buffer, pH 8.0. Ability to hydrolyse BHET (Sigma Aldrich, Product Code 465151) was determined by incubating 250 µM BHET with 1 µM enzyme at 60 °C, for either 4 h, or 12 h. Reverse-phase HPLC was used to quantify degraded species on a Shimadzu HPLC workstation using previously described methods [Yoshida et al., 2016].

3. Results and discussion:

3.1 Bioinformatics-based determination of Tf C residues crucial for PET binding

Figure 1A shows a *Tf* C-2HE-$(MHET)_3$ complex. Hydrophobic, electrostatic, hydrogen bonding and van der Waals interactions between *Tf* C and 2HE-$(MHET)_3$ in this docked structure are illustrated in Figure 1B. Residues observed to participate in interactions with 2HE-$(MHET)_3$ were confirmed using Molecular Dynamics (MD) simulations. The MD simulation interaction diagram (SID) is shown in Figure 1C, plotting fraction/extent of interactions during 75 ns simulations. With PETase (PDB ID: 6ANE) [Fecker et al., 2018], and LCC (PDB ID: 4EB0) [Sulaiman et al., 2012], respectively, *Tf* C (PDB ID: 4CG1) [Roth et al., 2014] shows RMSD alignment values of ˜1.26 Å, and ˜1.04 Å. We compared *Tf* C's structure with those of PETase, and LCC, in respect of analogous residues (in and around the active site) that make contact with 2HE-$(MHET)_3$ in docking and MD studies, to decide upon mutations of *Tf* C residues into residues present at structurally-analogous locations in PETase, or LCC, with a view to examining the effect of such mutations upon *Tf* C's activity. Notably, this approach is analogous to recent work in which residues in PETase were replaced by residues in *Tf* C [Fecker et al., 2018]. Our objectives were (i) to obtain mutants/variants superior to *Tf* C, and (ii) to analyse reductions or improvements in activity, in light of mechanistic and catalytic insights.

The mutants made are listed below. **G62A** : G62 is located in the PET-binding groove (Figure 1A). Mutation G62A reduces inhibition of *Tf* C by MHET and increases activity by ˜2.0-fold [Wei et al., 2016], ostensibly through disruption of steric clashes preventing interactions (required for release of product after hydrolysis) of residue G59's backbone nitrogen atom with a carbonyl oxygen in PET. We used G62A as a control, and also as a background (base) mutation for other mutations. **L90A, L90F** (F125 in LCC, otherwise conserved): L90 is distal to *Tf* C's PET binding groove (Figure 1A and Supporting Information Figure S1). L90A shows a 5-fold increase in activity upon cutin, over *Tf* C [Dong et al., 2020]. Mutations L90A and L90F were made to examine effects on activity. **H129W** (W132 in PETase [Fecker et al., 2018]): PETase is more catalytically active than *Tf* C between 30 and 40 °C. To mimic PETase's catalytic environment around S130 in *Tf* C, mutation H129W was performed (Supporting Information Figure S2A), in place of H129A, already reported to reduce PET hydrolysis by 80% [Fecker et al., 2018]. **W155F** (W conserved in all PET hydrolases), **H184A, and H184S** (S187 in PETase): These mutations were made with a view to create more space in *Tf* C's OET/PET-binding cleft towards more efficient PET binding (Supporting Information Figure S2A). H184 was made to allow a nearby tryptophan to wobble between open and closed conformers, as in PETase [Han et al., 2017]. **A173C/A210C** (C174/C210 in PETase) and **A173C/A206C** : These mutations were jointly made to create a disulphide bond below *Tf* C's catalytic site, mimicking such a bond in PETase [Han et al., 2017], to study its role in catalysis (Supporting Information Figure S2B). **Δ˜164** : V164 exists in a loop following a beta strand leading to D176 (a member of *Tf* C's catalytic triad). This was deleted to bring D176 closer to the other two residues in the triad, to promote better catalysis by minimizing distance between D176 and H208 (Supporting Information Figure S3).**F209I** (S211 in PETase), **F249R** , and **F249A** (not conserved): These residues lie either near or somewhat away from *Tf* C's active site. Mutations were made to reduce surface hydrophobicity without compromising catalysis (Supporting Information Figure S1).

General : L90, F209 and F249 (Figure 1A), were mutated to either increase hydrophobicity (e.g., L90F) or reduce it (e.g., F209I, F249R). Other residues shown in red (Figures 1B and 1C) were mutated to gain mechanistic insights.

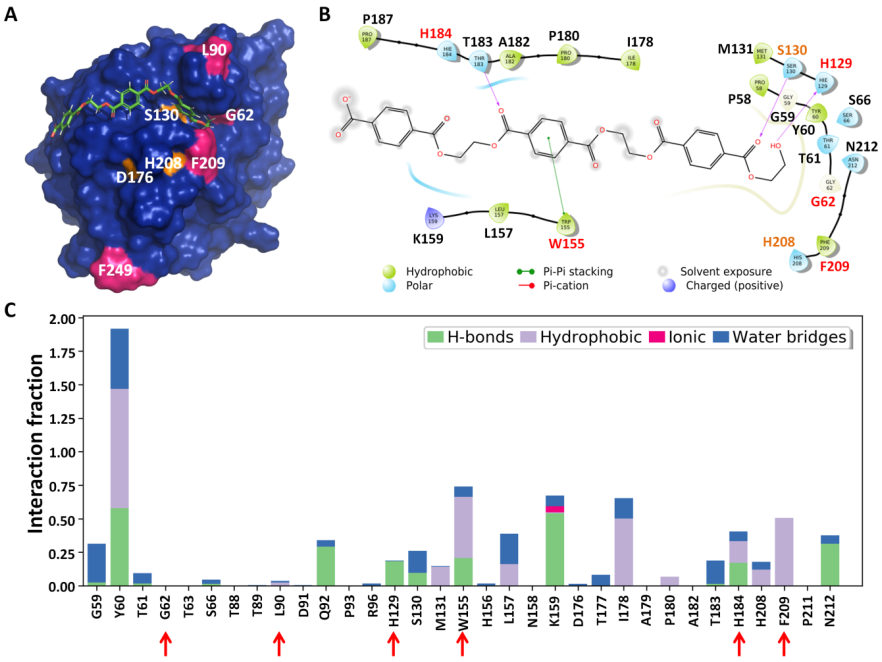

Figure 1: Molecular docking and molecular dynamics simulations of *Tf* C and 2HE-$(MHET)_3$. (A) Surface representation of *Tf* C docked with 2HE-$(MHET)_3$, showing catalytic triad residues in orange and potential regions selected for altering PET binding affinity shown in pink. Residues in *Tf* C participating in interaction with 2HE-$(MHET)_3$obtained from (B) Molecular docking and (C) Molecular dynamics simulations performed for 75 ns.

3.2 Activity assessments of various Tf C mutants upon PET and BHET

Figure 2A compares activities of mutants and *Tf* C against commercially-sourced PET (film). G62A was ˜1.7-fold more active than *Tf* C, corroborating its reported ˜2.0-fold higher activity [Wei et al., 2016]. D12L, and E47F, designed to enhance surface hydrophobicity at regions distal to the substrate-binding site, showed activity levels similar to that of *Tf* C. W155F, H184S, H184A, and F209S, designed to create more space at or near PET binding sites, and H129W, designed to increase hydrophobicity (in imitation of PETase), showed drastic reductions in activity against PET, indicating that mutations in the active site impact catalysis negatively, through changes in binding site geometry that are not tolerated, despite conservation of overall enzyme fold. Importantly, a previous study showed higher (rather than lower) activity in H129W [Furukawa et al., 2019]. Since *Tf* C contains S136 as a vicinal residue of H129W, and S136 happened to be T136 in our *Tf* C clone, we mutated T136 to S136 to create H129W/T136S which, however, also showed lower (rather than higher) activity, in contradiction of the earlier report. We propose that H129 influences catalysis in a previously-unsuspected manner.

W155F and H184S were non-active against commercial-sourced PET films of high crystallinity (˜250 microns thickness). Both mutants, however, showed activity against thin PET films of low crystallinity (˜10 microns thickness), made through dissolution of PET granules (each of ˜30 mg) and evaporation of the solvent (HFIP), on the walls of a micro-centrifuge tube. Interestingly, using such thin films, A173C showed ˜40% improvement over *Tf* C. However, using commercially-sourced PET films, A173C was 30% less active than *Tf* C, suggesting differences in how these enzymes see PET backbones in films of different thickness and crystallinity. A173

is situated just below the 'catalytic triad' residues D176 and H208 (Supporting Information Figure S2B). The A173C mutation could be anticipated to decrease space in the binding cleft, facilitating better catalysis upon thin PET films containing accessible PET chains (Supporting Information Figure S4) but giving rise to poorer catalysis with crystalline or semi-crystalline (thicker) commercial PET films (Figure 2A) at the reaction temperature of 60 @C. A173C/A210C, and A173C/A206C, created to introduce a disulphide bond below the catalytic cleft (mimicking such a bond in PETase) led to loss of activity, suggesting distortion of *Tf* C's binding site. Deletion of V164 in a loop connecting β-strands below the active site also led to loss of activity.

L90, situated distal to the binding site, was mutated to A90 (less hydrophobic), and also to F90 (more hydrophobic), analogous to F125 in LCC. L90A showed reduced activity upon PET (data not shown). In contrast, G62A/L90F showed a ˜2.3-fold increase in activity, compared to *Tf* C. G62A/F209I (corresponding to F243I variant of LCC [Tournier et al., 2020]), showed a ˜3.17-fold improvement. The variant G62A/F249R showed the highest hydrolytic potential against commercial-sourced PET films, with a ˜3.5-fold improvement over *Tf* C. G62A/F209I and G62A/F249R are anticipated to show reduced PET binding, due to the replacement of phenylalanine by a less hydrophobic residue, or a charged residue. This may allow a higher fraction of the *Tf* C population to remain in solution and, therefore, to act upon degradation intermediates accumulating in solution, so as to function synergistically with the bound enzyme fraction of *Tf* C (invading and degrading solid PET), to generate TPA. This could explain the enhancement of activity in these two variants, through a reduction in non-specific PET binding, or faster dissociation from PET, without any alterations in the active site.

Most mutants showing loss of activity against commercial PET film also showed reduced catalytic degradation of BHET. In Figure 2B, H129W shows the least activity with BHET, with H129W/T136S showing improved degradation of BHET into TPA. L90A and A173C/A206C showed BHET hydrolysis comparable to *Tf* C. This suggests that the inability of these mutants to degrade PET owes to compromised PET-binding, and not to compromise hydrolysis of ester bonds. The G62A variant along with four other binding-altered variants made using G62A as background (i.e., G62A/L90F, G62A/F209I, G62A/F249A and G62A/F249R) showed ˜1.6 to ˜2.0-fold improvements in conversion of BHET into TPA. The mutants showed similar relative trends in their ability to hydrolyse BHET over 12 h (Figure 2B) or 4 h (Supporting Information Figure S5). F209I showed maximum enhancement of BHET conversion, ˜2 fold higher than *Tf* C after 12 h of incubation.

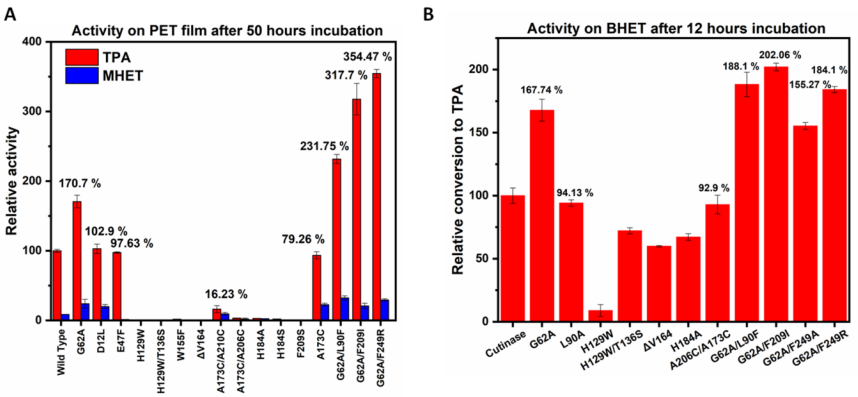

Figure 2: Comparison of activity of various *Tf* C mutants with respect to *Tf* C, against (A) commericial PET films, (B) BHET. The error bars show standard deviation based on tripicate measurements.

3.3 Spectroscopic, chromatographic and PET-binding characteristics of mutants.

Tf C is an α/β hydrolase which shows a CD spectrum typical of proteins with mixed α/β structures, with a spectral shape dominated by negative bands at 208 and 222 nm, and spectral intensity characterized by

substantially lower MRE than is associated with α-helices. CD spectra of all mutants/variants overlapped substantially with that of*Tf* C, demonstrating that the enzyme tolerated the mutations, and remained folded in a native-like structural format (Figure 3A). Size exclusion chromatographic behaviour of all mutants/variants was identical to that of *Tf* C, with elution occurring at the same volume (˜13.5 ml) from the column used (data not shown for all mutants in Figure 3B). Only L90F eluted at a later volume (˜14.1 ml), due to hydrophobic interactions with the column matrix, owing to the enhanced surface hydrophobicity (Figure 3B).

We performed PET-binding assays, based on SDS-PAGE analyses of enzyme populations seen in lanes corresponding to reaction supernatants, or extracts of PET-bound populations (Figure 3C), followed by densitometric analyses (Figure 3D). These assays were performed for mutants/variants, G62A/L90F, G62A/F209I and G62A/F249R. Binding of L90F to PET was noted to be comparable to that of *Tf* C, in that the partitioning of enzyme populations between PET (lane 1 *versus* lane 3) and solution (lane 2 *versus* lane 4) were similar. In contrast, with the G62A/F209I variant, significantly less enzyme was seen to have remained bound to PET (lane 6 and Figure 3D), with proportionate increase in the enzyme left in solution (lane 7). Figure 3D shows that PET binding by G62A/F249R is intermediate to that of G62A/L90F and G62A/F209I. The differences would appear to owe to differences in overall surface hydrophobicity, wrought through the protein engineering carried out.

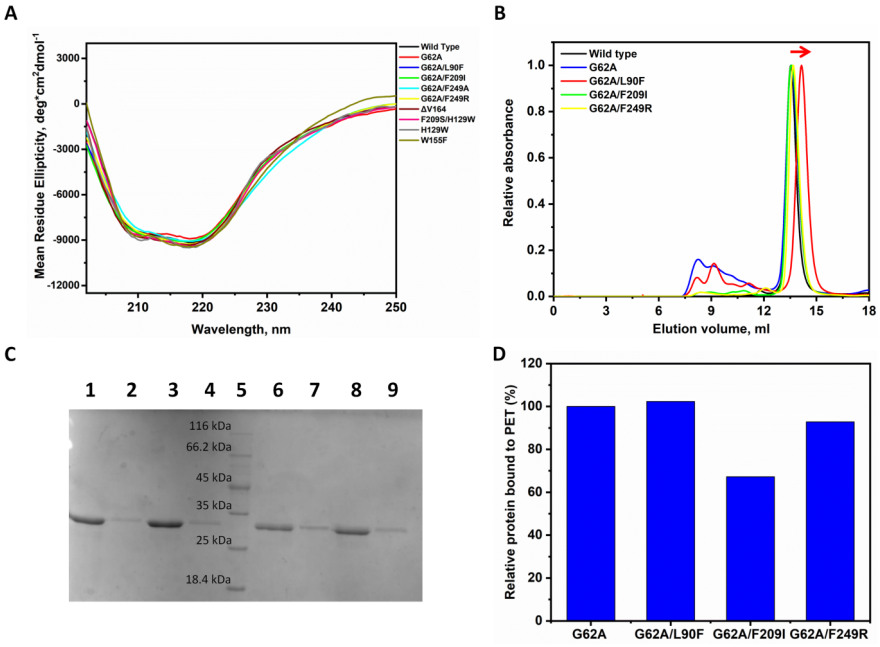

Figure 3: (A) Secondary structure assessment for *Tf* C and different mutants. (B) Size exclusion chromatography of binding altered variants of *Tf* C. (C) SDS-PAGE analysis for partitioning of *Tf* C after 40 h incubation with PET film. Lane 1: G62A bound to PET, Lane 2: G62A in solution, Lane 3: G62A/L90F bound to PET, Lane 4: G62A/L90F in solution, Lane 5: Protein marker, Lane 6: G62A/F209I bound to PET, Lane 7: G62A/F209I in solution, Lane 8: G62A/F249R bound to PET, Lane 9: G62A/F249R in solution. (D) Densitometric quantification of proteins in lanes 1, 3, 6, 8.

3.4 Thermal and chemical (kinetic and thermodynamic) stability of Tf C

Thermal unfolding of *Tf* C was examined using CD and DSC. Changes in *Tf* C's secondary structure were measured during heating (20 °C to 90 °C), at 1 °C/min, and 0.2 °C/min, respectively (Figure 4A). At the faster unfolding rate of 1 °C/min, ˜70% denaturation was observed at 90°C, whereas at the slower unfolding

rate of 0.2 °C/min, ~100 % unfolding was observed, with a T_m of ~85 °C. This indicates that *Tf* C is kinetically (thermally) stabilized, displaying a resistance to unfolding that leads to unfolding equilibrium being achieved only through slower heating. To further *Tf* C's unfolding kinetics, changes in CD were monitored over 120 min incubations, at temperatures flanking the T_m (Figure 4B). The Arrhenius plot obtained from rates of unfolding in the range of 68-87.5 °C (Supporting Information Figure S6A) yielded an activation energy, E_a, of 217.557 kJ/mol (i.e. 52 kcal/mol). Thermodynamic parameters determined through construction of an Eyring plot (Supporting Information Figure S6B) were: (1) ΔH = 214.643 kJ/mol; (2) ΔS = 314.4346 J/mol*K; and (3) ΔG = 120.96 kJ/mol (i.e. 28.9 kcal/mol). DSC measurements (Figure 4C) corroborated the T_m determined by CD, while establishing two proximal unfolding transitions at ~78.5 °C and ~86.7 °C, supporting the high thermal, kinetic, and thermodynamic stability of *Tf* C, and causing *Tf* C to be suited to PET degradation at temperatures close to PET's glass transition temperature over hours, or tens of hours. *Tf* C's chemical stability was explored through overnight incubation in urea (0 to 8 M), or guanidium hydrochloride, Gdm.HCl (0 to 6M), based on measurements of changes in the CD signal at 222 nm. *Tf* C is resistant to urea, but not to Gdm.HCl (Figure 4D), which is a more potent denaturant (disrupting electrostatic interactions and hydrogen bonding, unlike urea which primarily disrupts only hydrogen bonding). Gdm.HCl causes unfolding with an apparent $C_m$of 3.9 M. Kinetics of denaturation by Gdm.HCl were determined through 2 h incubations of *Tf* C at 5M, 5.5M, 6M, 6.5M and 7M Gdm.HCl (Figure 4E). The rate of unfolding in absence of denaturant, $K_{u,w}$, was determined from a half-chevron plot (Supporting Information Figure S7), to be $3.77*10^{-11}s^{-1}$, indicative of slow unfolding. This resistance to thermal and chemical denaturation bodes well for *Tf* C's utility under industrial conditions.

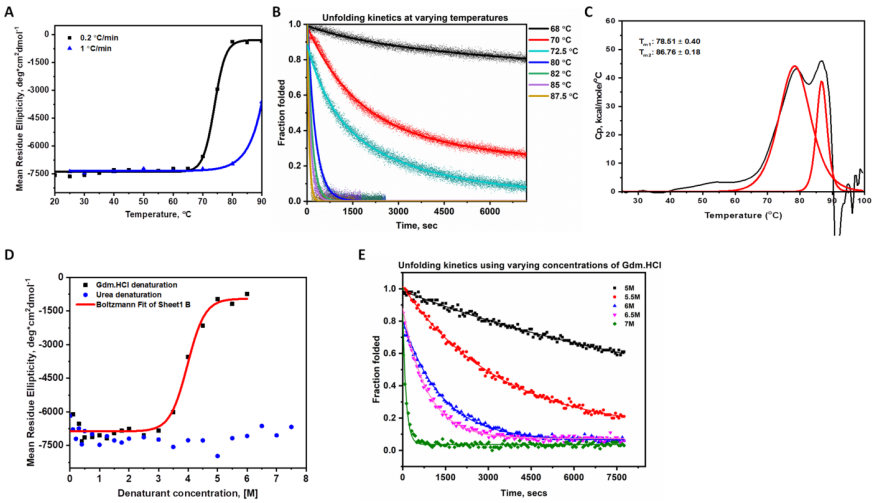

Figure 4: Thermal and chemical denaturation studies. (A) MRE at 222 nm at temperatures from 20 °C to 90°C at rates of 0.2 °C/min and 1 °C/min , measured by CD. (B) Thermal kinetics demonstrating fraction folded during 2 hour incubations at different temperatures (68 °C to 87.5 °C), measured by CD. (C) DSC showing two-transition unfolding of *Tf* C. (D) MRE at 222 nm at varying urea (0 M to 8 M) and GdmCl (0 M to 6 M) concentrations, measured by CD. (E) Chemical kinetics demonstrating fraction folded during 2 h incubations at different concentrations of GdmCl (5 M to 7 M), measured by CD.

4. Conclusions:

We created 17 mutants of *Tf* C, with a view to (a) creating or removing space in the active site, to modulate catalysis, or (b) increasing or decreasing hydrophobicity in-and-around the binding site, or at distal locations, to modulate *Tf* C's binding of PET. In every instance attempting to alter catalytic efficiency through changes made to residues at the active site, we only observed a reduction or complete abolition of activity upon solid PET, sometimes without a reduction in activity against BHET, indicating the sensitivity of *Tf* C's active

site to binding to crystalline PET chains. In stark contrast, we achieved significant success with mutations designed to reduce non-specific (hydrophobic) interactions of *Tf* C with PET, at locations distal to the active site, where our intention was to facilitate either (i) improved dissociation of enzyme from PET, following catalysis, to free up enzyme for further rounds of binding and catalysis, or (ii) the improved presence of enzyme in solution, to concomitantly convert OETs, BHET or MHET into TPA. Mutants G62A/F209I, G62A/F249R, and G62A/L90F displayed between ˜2.3-fold and ˜3.0-fold enhancement in PET degradation over *Tf* C, and between ˜1.3-fold and ˜2.0-fold enhancement over G62A *Tf* C, which is known to be the currently best-performing mutant/variant of *Tf* C.

Acknowledgements: AM thanks DBT, India, and HK and BT thank CSIR, India, for doctoral fellowships. MP was a Masters' thesis student. PG thanks DBT, India, for grant BT/PR/31706/PBD/26/705/2019. The work was mainly conceived and executed by AM under the supervision of PG, and the first draft was written up by AM and then edited by AM and PG. MP and HK worked under the immediate supervision of AM and the overall supervision of PG. MP produced and studied four of the seventeen mutants. HK worked with AM in determining the activities of mutants against BHET and PET. BT participated in discussions about the work, suggested the making of certain mutants, and helped with trouble-shooting in the production of genes/proteins in respect of several mutants.

Declaration of conflicting interests: The authors have no conflicting interests.

Supplementary Data: The seven figures in the supplementary data for this article can be viewed online.

References

Buchholz, P. C. F., Feuerriegel, G., Zhang, H., Perez-Garcia, P., Nover, L. L., Chow, J., Streit, W. R., & Pleiss, J. (2022). Plastics degradation by hydrolytic enzymes: The plastics-active enzymes database—PAZy. *Proteins: Structure, Function and Bioinformatics* , 1443–1456.

Dong, Q., Yuan, S., Wu, L., Su, L., Zhao, Q., Wu, J., Huang, W., & Zhou, J. (2020) Structure-guided engineering of a *Thermobifida fusca* cutinase for enhanced hydrolysis on natural polyester substrate. *Bioresources and Bioprocessing* . *7* (1), 37.

Ellis, L.D., Rorrer, N.A., Sullivan, K.P., Otto, M., McGeehan, J.E., Román-Leshkov, Y., Wierckx, N., & Beckham, G.T. (2021) Chemical and biological catalysis for plastics recycling and upcycling. *Nature Catalysis* , *4* (7), 539–556.

Fecker, T., Galaz-Davison, P., Engelberger, F., Narui, Y., Sotomayor, M., Parra, L.P., & Ramírez-Sarmiento, C.A. (2018) Active Site Flexibility as a Hallmark for Efficient PET Degradation by *I. sakaiensis* PETase. *Biophysical Journal* , *114* (6) 1302–1312.

Furukawa, M., Kawakami, N., Tomizawa, A. & Miyamoto, K. (2019) Efficient Degradation of Poly(ethylene terephthalate) with *Thermobifida fusca* Cutinase Exhibiting Improved Catalytic Activity Generated using Mutagenesis and Additive-based Approaches. *Scientific Reports* , *9* (1) 1–9.

Geyer, R., Jambeck, J.R., & Law, K.L. (2017) Production, use, and fate of all plastics ever made. *Science Advances* , *3* (7), 25–29.

Han, X., Liu, W., Huang, J.W., Ma, J., Zheng, Y., Ko, T.P., Xu, L., Cheng, Y.S., Chen, C.C., & Guo, R.T. (2017) Structural insight into catalytic mechanism of PET hydrolase. *Nature Communications* ,*8* (1), 2106.

Jensen, K., Borch, K., Westh P., & Kari, J. (2022) Sabatier Principle for Rationalizing Enzymatic Hydrolysis of a Synthetic Polyester .*JACS Au* , *2* (5), 1223–1231.

Kawai, F., Kawabata T., & Oda, M. (2019) Current knowledge on enzymatic PET degradation and its possible application to waste stream management and other fields. *Applied Microbiology and Biotechnology* ,*103* , 4253-4268.

Kawai, F., Kawabata, T., & Oda, M. (2020) Current State and Perspectives Related to the Polyethylene Terephthalate Hydrolases Available for Biorecycling. *ACS Sustainable Chemistry & Engineering* , *8* (24), 8894–8908.

Maurya, A., Bhattacharya, A., & Khare, S.K. (2020) Enzymatic Remediation of Polyethylene Terephthalate (PET)–Based Polymers for Effective Management of Plastic Wastes: An Overview. *Frontiers in Bioengineering and Biotechnology* , *8* , 1–13.

Mrigwani, A., Thakur B. and Guptasarma, P. (2022) Enhancing high-temperature degradation of polyethylene terephthalate through a synergistic division of enzyme labour between a solid-degrading thermostable cutinase and a reaction intermediate-degrading thermostable carboxylesterase, *BioRxiv*https://doi.org/10.1101/2022.02.02.478778

Roth, C., Wei, R., Oeser, T., Then, J., Föllner, C., Zimmermann, W., Sträter, N. (2014) Structural and functional studies on a thermostable polyethylene terephthalate degrading hydrolase from *Thermobifida fusca* . *Applied Microbiology and Biotechnology* . *98* (18) 7815-23.

Ru, J., Huo, Y., & Yang, Y. (2020) Microbial degradation and valorization of plastic wastes. *Frontiers in Microbiology* ,*11* , 442.

Sarah, K., & Gloria, R. (2021) Achieving a circular bioeconomy for plastics. *Science*, *37*, 49-50.

Sulaiman, S., Yamato, S., Kanaya, E., Kim, J.-J, Koga, Y., Takano, K., Kanaya, S. (2012) Isolation of a novel cutinase homolog with polyethylene terephthalate-degrading activity from leaf-branch com- post by using a metagenomic approach. *Applied and Environmental Microbiology* , *78* , 1556-1562.

Sulaiman, S., You, D.J., Eiko, K., Koga, Y., Kanaya, S. (2012) Crystal structure of Leaf-branch compost bacterial cutinase homolog. PDB DOI: 10.2210/pdb4EB0/pdb

Tournier, V., Topham, C.M., Gilles, A., David, B., Folgoas, C., Kamionka, E., Desrousseaux, M., Texier, H., Gavalda, S., Cot, M., Guemard, E., Dalibey, M., Nomme, J., Cioci, G., Barbe, S., Chateau, M., Andre, I., Duquesne, S., & Marty, A. (2020) An engineered PET depolymerase to break down and recycle plastic bottles. *Nature* ,*580* , 216–219.

Wei, R., Oeser, T., Schmidt, J., Meier, R., Barth, M., Then J., & Zimmermann, W. (2016) Engineered bacterial polyester hydrolases efficiently degrade polyethylene terephthalate due to relieved product inhibition. *Biotechnology and Bioengineering* , *113* (8), 1658–1665.

Wei, R., von Haugwitz, G., Pfaff, L., Mican, J., Badenhorst, C.P.S., Liu, W., Weber, G., Austin, H.P., Bednar, D., Damborsky, J., & Bornscheuer, U.T. (2022) Mechanism-Based Design of Efficient PET Hydrolases. *ACS Catalysis* , *12* (6), 3382–3396.

Yoshida, S., Hiraga, K., Takehana, T., Taniguchi, I., Yamaji, H., Maeda, Y., Toyohara, K., Miyamoto, K., Kimura, Y., Oda, K. (2016) A bacterium that degrades and assimilates poly(ethylene terephthalate).*Science* , *351* , 1196-1199.

Zhang, Y. & Skolnick, J. (2005) TM-align: a protein structure alignment algorithm based on the TM-score. *Nucleic Acids Research* ,*33* , 2302e2309.